

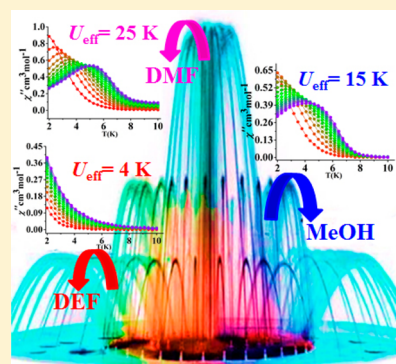
Sizeable Effect of Lattice Solvent on Field Induced Slow Magnetic Relaxation in Seven Coordinated Co^{II} Complexes

Arpan Mondal, Ajit Kumar Kharwar, and Sanjit Konar*[✉]

Department of Chemistry, Indian Institute of Science Education and Research Bhopal, Bhopal Bypass Road, Bhauri, Bhopal 462066, MP, India

Supporting Information

ABSTRACT: We have demonstrated the effect of a solvent at the second coordination sphere on slow relaxation of magnetization for hepta-coordinated cobalt(II) complexes with the formulas [Co(H₄L)(DMF)(H₂O)](NO₃)₂·(DMF) (1), [Co(H₄L)(MeOH)(H₂O)](NO₃)₂·(MeOH) (2), and [Co(H₄L)(DEF)(H₂O)](NO₃)₂ (3) (H₄L = 2,2'-(pyridine-2,6-diylbis(ethan-1-yl-1-ylidene))bis(*N*-phenylhydrazinecarboxamide)). Structural analysis reveals that the presence of lattice solvent molecule in 1 and 2 dramatically changes the crystal packing and noncovalent interactions as compared to 3 where no solvent molecule is present in the crystal lattice. The dc and ac magnetic susceptibility measurements reveal the presence of easy-plane magnetic anisotropy for all the complexes, and field induced slow relaxation behavior has been observed above 2 K for 1 and 2 in contrast to 3 due to the availability of the solvent molecules in the crystal lattice. The *ab initio* calculations further support the sign of *D* and the negligible effect of the first co-ordination sphere, as almost similar *D* values were obtained for all the complexes. The field and temperature dependence of relaxation time confirm that quantum tunnelling of magnetization (QTM) plays a major role in slow magnetic relaxation, and thermal dependence like an optical or acoustic Raman pathway is also important. To further analyze the effect of dipole–dipole interaction on slow magnetic relaxation, a dilution experiment has been performed.



INTRODUCTION

In the field of molecular magnetism, single-molecule magnets (SMMs)¹ have attracted considerable attention, as their magnetic bistability can be used as a prospective component for molecular spintronics,² high information storage, and quantum computing.³ After the discovery of SMM behavior of Mn₁₂, more efforts were dedicated to prepare the multinuclear complexes with a large spin ground state to get a high energy barrier for slow magnetic relaxation.⁴ However, this strategy was not very successful because in a multinuclear system the different orientation of the resultant magnetization vector reduces the anisotropy, which must be large to observe better SMM behavior.^{4c,d} On the other hand, the complexes with one paramagnetic metal center, referred to as single ion magnets (SIMs), are relatively easier in terms of controlling the anisotropy, having a high energy barrier (*U*_{eff}) and blocking temperature (*T*_B).^{4,5} In addition, substantial effort has been spent in optimization of uniaxial anisotropy of these molecules with a minimum rhombic term by applying a proper ligand field and suitable geometry around the metal centers. Recently, the highest hysteresis temperature found was 80 K for a two coordinated dysprosium metallocene complex reported by Gao et al.^{5f} The observed high hysteresis temperature is close to liquid nitrogen temperature, bringing hope for real application prospects in the future. Besides the lanthanides, transition metal complexes also display interesting SMM behavior in a proper ligand field and geometry as the ligand field is much

more effective for 3d metal ions.⁶ Considering all the reported 3d-based SIMs, the most demanding feature is a low coordination number of the metal center as the anisotropy is enhanced due to unrestricted orbital angular momentum. In this regard, Co^{II} complexes are the most desirable candidates for SIMs⁷ because of their large magnetic anisotropy and noninteger spin ground state, which reduce the possibility of quantum tunneling of magnetization (QTM).^{6h–k,8} Recently, Bunting et al. reported the highest spin reversal barrier of 450 cm⁻¹ among transition metal complexes for a linear two coordinated cobalt complex with maximal orbital angular momentum.^{8c} As low coordinated cobalt complexes are not stable, more efforts have been made to tune their geometry to enhance their magnetic anisotropy.^{8,9} However, hepta-coordinated Co^{II} SIMs with pentagonal bipyramidal (PBP) geometry are still limited where only the effect of coordination environment on easy-plane magnetic anisotropy has been studied.¹⁰ The spin–orbit coupling between ground electronic states with two excited electronic states results in the easy-plane magnetic anisotropy for those systems. Thus, the anisotropy can be tuned by changing the extent of mixing between ground and excited states with proper ligand field. In our previous report on Co^{II}–PBP complexes, we showed that weak sigma donor ligand can increase the magnitude of the

Received: March 2, 2019

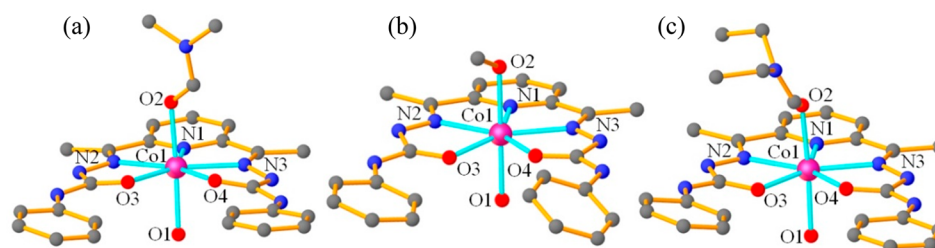


Figure 1. View of molecular structure for complexes 1–3 (a–c). Solvent molecules and H atoms are omitted for clarity.

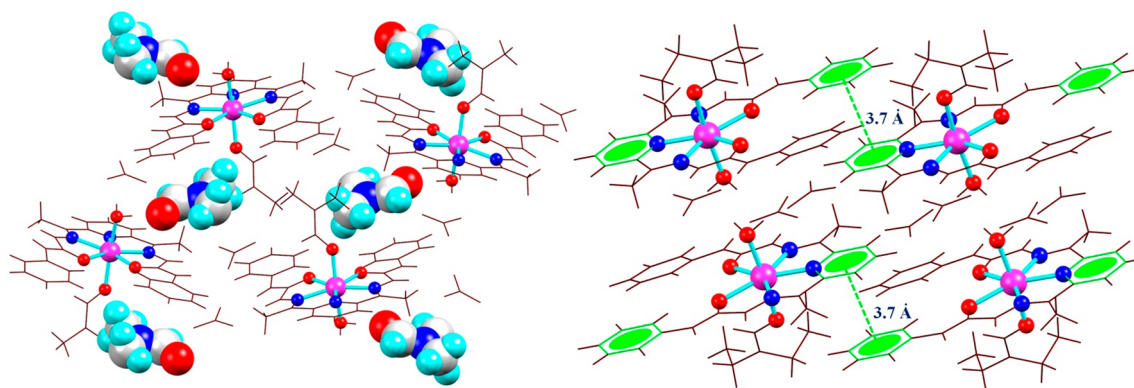


Figure 2. Crystal packing diagram of complexes 1 (left) and 3 (right) along the crystallographic *b* axis.

anisotropy parameters (*D*-axial and *E*-rhombic anisotropy) as well as energy barrier.^{9c} However, all methods can be summed up in two aspects which have been used to increase the energy barrier and blocking temperature: first, regulating the coordination and geometry around metal center; second, accepting suitable counterions or solvents. Usually, the magnetization reversal is highly sensitive toward the first coordination sphere, local symmetry, and single ion anisotropy of the metal center.^{6,7,11} At the same time, the solvent molecule present in the crystal lattice may lead to different dipole–dipole interactions, which controls the relaxation rate of incoherent quantum tunneling and results in a drastically different energy barrier of magnetization reversal.¹² Thus, the lattice solvent may also play an important role in relaxation dynamics.

In this work, we have reported the first example of Co(II) SIMs with PBP geometry with the formulas $[\text{Co}(\text{H}_4\text{L})(\text{DMF})(\text{H}_2\text{O})](\text{NO}_3)_2 \cdot (\text{DMF})$ (**1**), $[\text{Co}(\text{H}_4\text{L})(\text{MeOH})(\text{H}_2\text{O})](\text{NO}_3)_2 \cdot (\text{MeOH})$ (**2**), and $[\text{Co}(\text{H}_4\text{L})(\text{DEF})(\text{H}_2\text{O})](\text{NO}_3)_2$ (**3**) ($\text{H}_4\text{L} = 2,2'$ -(pyridine-2,6-diylbis(ethan-1-yl-1-ylidene))-bis(*N*-phenylhydrazinecarboxamide), where lattice solvent plays an important role in the slow relaxation of magnetization.

RESULTS AND DISCUSSIONS

Structural Description. From the single crystal X-ray analysis, it has been observed that complexes **1** and **2** (Figure 1) crystallize in monoclinic $P2_1/c$ and $P2_1$ (Table S1) space groups, whereas complex **3** (Figure 1) crystallizes in the triclinic $P\bar{1}$ space group (Table S1). All the complexes have a N_3O_4 coordination environment where the H_4L ligand binds with the Co^{II} center equatorially by five donor sites, leaving the axial position free for the solvent and water molecules. The charge of the metal center is balanced by the nitrate counterions, which are strongly hydrogen bonded with the coordinated water (Figure S1 and Table S2) and the

neighboring molecules in all the complexes. The asymmetric unit contains one Co^{II} ion and one molecule of water in the axial position for all complexes. The other axial position is occupied by solvent molecules DMF, MeOH, and DEF in complexes **1**, **2**, and **3**, respectively. Even under a similar ligand field environment, the equatorial coordination shows little difference [ligand bite angles from 69.72° (for Npyridyl–Co–N) to 77.97° (for O–Co–O) in complex **1**, compared to 70.96 – 74.51° and 70.39 – 76.99° for the equivalent angles in **2** and **3**, respectively] (Table S3). The free –NH group of the ligand is strongly hydrogen bonded to the free nitrate anions present in the crystal lattice (Figure S2 and Table S2) of all the complexes. In addition, one free solvent molecule (DMF in complex **1** and MeOH in complex **2**) is present in the asymmetric unit, which is strongly hydrogen bonded with the axial water molecules, whereas in **3**, the same hydrogen bond is observed only by the nitrate anion (Figure S1). In complex **3**, no free solvent molecule is present in the crystal lattice. The presence of the lattice solvent in **1** and **2** dramatically changes the crystal packing (Figures 2, S3, and S4) as compared to **3**, which shows alternative π – π interaction (3.71 Å) in the crystal packing (Figures 2 and S5). Interestingly, the π – π interactions are totally absent in the former complexes (**1** and **2**). Further, the analysis of the crystal packing reveals that the nearest Co–Co distance is in the range of 8.13–9.34 Å for all complexes. The continuous shape measurements (CShM),¹³ used to calibrate the deviation of the structures from the reference polygons, were calculated to be 0.293, 0.067, 0.253 for **1**–**3**, respectively, which are very close to zero of the ideal D_{5h} geometry. Complete results of the geometric analyses are shown in Tables S3, S4, and S5.

Magnetic Property Studies. The magnetic susceptibility measurements were performed under an applied field of 0.1 T in the temperature range of 2–300 K. For all the complexes, the purity of the bulk sample was confirmed by the powder X-ray diffraction data compared to the simulated ones (Figure

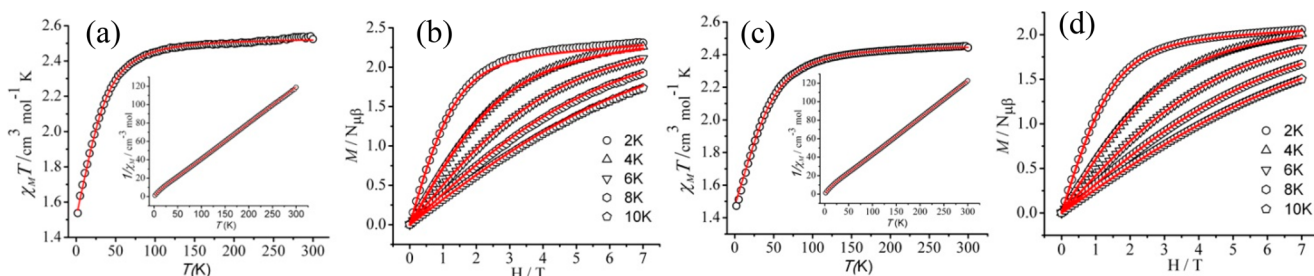


Figure 3. $\chi_M T$ vs T plots measured at 0.1 T for complex 1 (a) and 3 (c). The $1/\chi_M$ vs T plots are shown in the inset. $M/N\mu_B$ vs H plots for 1 (b) and 3 (d) at the indicated temperatures. The red lines are the best fit.

S6). At room temperature, the $\chi_m T$ values (χ_m = molar magnetic susceptibility) were obtained as 2.52, 2.47, and 2.44 $\text{cm}^3 \text{mol}^{-1} \text{K}$ for complexes 1–3 (Figures 3 and S7), respectively. These values are slightly higher than the spin only value (1.87 $\text{cm}^3 \text{mol}^{-1} \text{K}$, $g = 2.0$) for the noninteracting Co^{II} high spin ion, but they fall within the usual range of 2.1–3.4 $\text{cm}^3 \text{mol}^{-1}$ observed for highly anisotropic Co^{II} ions (where $g > 2.0$). Upon cooling the temperature from 300 K, the $\chi_m T$ value slowly decreases for all the complexes down to 110 K, below which it decreases rapidly and reaches a minimum value of 1.52(1), 1.5(2), and 1.42(3) $\text{cm}^3 \text{mol}^{-1} \text{K}$ at 2 K. The rapid decrease at low temperature is due to the presence of inherent anisotropy of the Co^{II} centers. In addition, the field dependence magnetization data have been collected, which reached the highest values of 2.26 (1), 2.15 (2), and 1.97 (3) at 7 T magnetic fields (Figures 3 and S7). The sharp increase of the magnetization at a low temperature (2 K) specifies the degenerate ground states, and at high field, (7 T) they become almost saturated, indicating the higher energy of the first excited states for all the complexes. Furthermore, the reduced magnetization curves (Figure S8) do not fall on the same master curve for all the complexes, showing the anisotropy of the system. Considering the large intermolecular distance (8.13–9.34 Å) between Co^{II} centers, the interaction between local spin quartets, if any, is expected to be very weak. Thus, the following spin Hamiltonian has been used to extract the ZFS parameter (D) as given in eq 1.^{10a–e}

$$H = g\mu_B S \cdot B + D[S_z^2 - S(S+1)/3] + E(S_x^2 - S_y^2) \quad (1)$$

In the above equation, axial and rhombic anisotropy parameters are represented by D and E respectively whereas other parameters have their usual meaning. The simultaneous fitting of $\chi_m T$ vs T and $M/N\mu_B$ vs H plots using the PHI program¹⁴ provides $D = 35.92 \text{ cm}^{-1}$, $|E| = 1.42 \text{ cm}^{-1}$, and $g = 2.3$ for 1; $D = 37.23 \text{ cm}^{-1}$, $|E| = 0.93 \text{ cm}^{-1}$, and $g = 2.29$ for 2; and $D = 43.76 \text{ cm}^{-1}$, $|E| = 0.84 \text{ cm}^{-1}$, and $g = 2.28$ for 3. In addition, the inclusion of the intermolecular interaction during the fitting shows very weak dipole–dipole interaction ($zJ = -0.025 \text{ cm}^{-1}$ for 1, $zJ = -0.013 \text{ cm}^{-1}$ for 2, and $zJ = -0.009 \text{ cm}^{-1}$ for 3) for all complexes. The obtained positive D values are in good agreement with previously reported Co^{II} PBP complexes.¹⁰ The fitting using a negative D value gives a poorer fit for all the complexes. The spin–orbit coupling between ground state and excited states results in a positive D value due to the electronic excitation between different m_l values of the d orbital as previously reported for hepta-coordinated Co^{II} complexes. To get further insight into the electronic structures and relaxation dynamics, we have studied *ab initio* calculations with the help of ORCA 4.0¹⁵ and MOLCAS 8.2 packages.¹⁶ In both calculations, the parameters

are in excellent agreement with those obtained from the fitting of the experimental data (Tables S6 and S7). It is also noticed that in all complexes the electronic transition occurs between the different m_l values of the d orbital (Figures 4 and S9), which results in the positive signs of the D parameters.

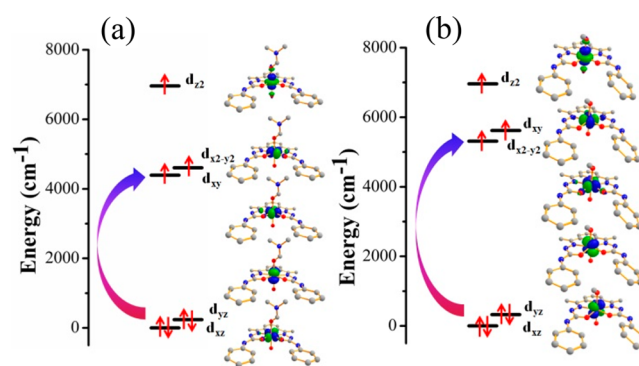


Figure 4. AILFT computed d-orbital splitting for complex 1 (a), 2 (b).

Additionally, the CASSCF/RASSI-SO/SINGLE_ANISO type calculations were performed by MOLCAS 8.2 where the orientation and easy plane type anisotropy are also observed in the ground Kramers doublet state (KDs; Figure S10 and Table S8) as the quartet $S = 3/2$ states splits further in two KDs $\pm 1/2$ and $\pm 3/2$. For all the complexes, the g tensor of the ground KDs is pretty close to the ideal values of $g_x = 6$, $g_y = 4$, and $g_z = 2$ for the $\pm 1/2$ type of the Kramers doublet (where $D > 0$, $E/D = 0$), which further aligns with the positive D value (Table S8). Also, the anisotropy of the first excited KDs is closer to the ideal values of $g_x = 0$, $g_y = 0$, and $g_z = 6$ for $\pm 3/2$ type KDs (Table S9). Thus, theoretical calculations also nicely produce the ZFS parameters (Tables S6 and S7) close to the experimental results, which further confirms the sign of ZFS parameters for all the complexes. The theoretically calculated D values are very close to each other as the coordination environments are almost similar in all complexes. To check the relaxation dynamics in complexes 1–3, alternating current (ac) susceptibility measurements have been performed under a 3.5 Oe ac field. None of the complexes show any frequency as well as temperature dependence in the absence of an external magnetic field. This may be due to the presence of fast resonant zero field quantum tunnelling of magnetization (QTM) between the ground KDs for all complexes. Thus, to reduce the QTM, we have applied 0.2 T as an optimal dc field (Figure S11). It was observed that out-of-phase (χ_M'') susceptibility shows a maximum value at 0.2 T almost for all complexes, and ac

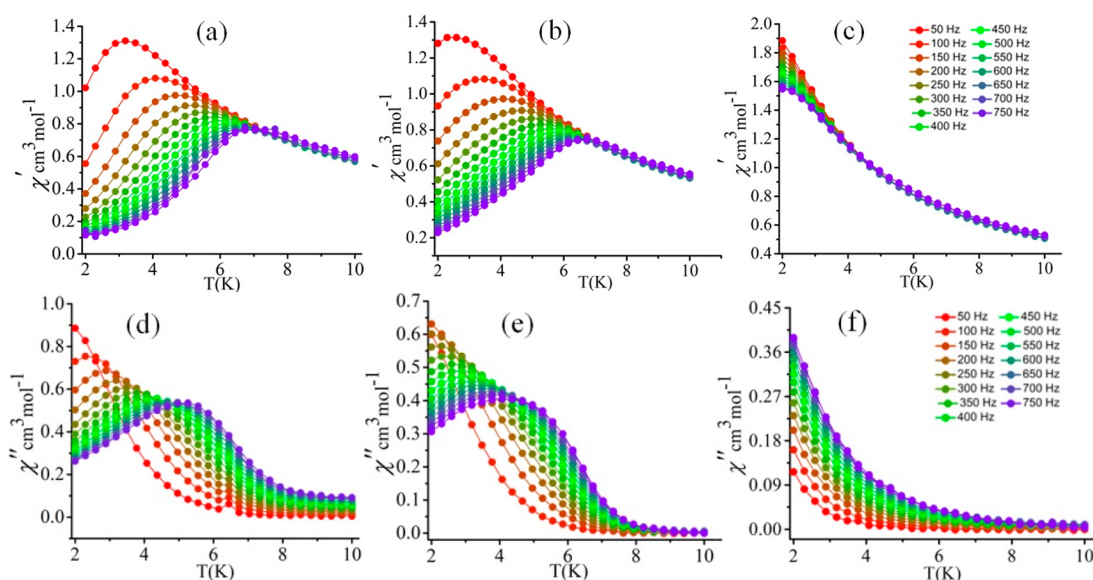


Figure 5. Temperature dependency of the in-phase (χ_M') for complex 1 (a), 2 (b), and 3 (c) and out-of-phase (χ_M'') 1 (d), 2 (e), and 3 (f) under a 0.2 T dc field.

measurements were performed under this external field. The complexes 1 and 2 show nice temperature (Figure 5) and frequency dependency (Figures S12 and S13). However, no such dependency is observed above 2 K for complex 3 (Figure 5). Additionally, the temperature dependence of in-phase (χ_M') and out-of-phase susceptibility (χ_M'') shows peak maxima below 2 K (Figure 5) for 3, which gives the indication of slow relaxation of magnetization. A generalized Debye model¹⁷ has been used to fit Cole–Cole plots (Figure 6) for 1

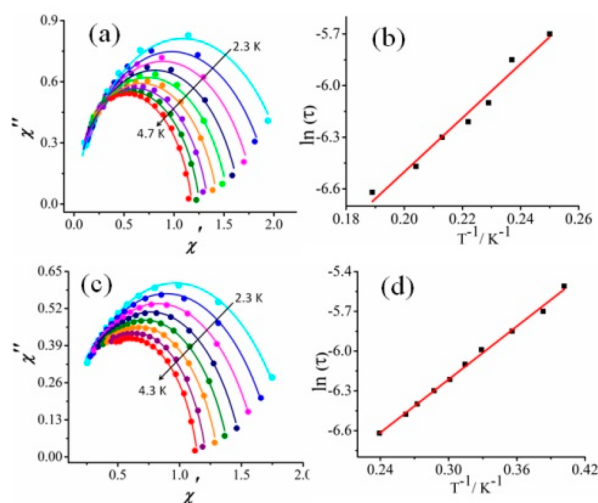


Figure 6. Cole–Cole plots for 1 (a) and 2 (c) and Arrhenius plots for 1 (b) and 2 (d). The solid lines represent the best fitting.

and 2 where the semicircle nature indicates a single relaxation process. The α (indicating the width of the distribution of relaxation time) values were obtained as 0.13–0.27 (1) and 0.09–0.26 (2), indicating the narrow distribution of the relaxation time. Further, to extract the energy of the magnetization reversal, the classical Arrhenius equation $\ln(\tau) = \ln(\tau_0) + U_{\text{eff}}/KT$ has been used (Figure 6) for 1 and 2 where clear peak maxima were observed above 2 K.^{6,8} The best fit gives the energy barrier (U_{eff}) and pre-exponential relaxation

time (τ_0) as $U_{\text{eff}} = 25$ K and $\tau_0 = 6.5 \times 10^{-6}$ s for 1 and $U_{\text{eff}} = 15$ K and $\tau_0 = 3.5 \times 10^{-6}$ s for 2. Since complex 3 does not show any peak maxima above 2 K, the Debye equation $\ln(\chi_M''/\chi_M') = \ln(\omega\tau_0) + U_{\text{eff}}/k_B T$ has been used to estimate the energy barrier (Figure S14). The linear fit of $\ln(\chi_M''/\chi_M')$ vs $1/T$ gives the energy barrier and pre-exponential relaxation time (τ_0) as $U_{\text{eff}} = 4$ K and $\tau_0 = 1.9 \times 10^{-6}$ s. For all complexes, the pre-exponential relaxation time is in the order of observed SIMs behavior (10^{-6} – 10^{-12}) as reported previously.^{6,7,10} Although, in 3d-SIMs with positive D , it is suggested that relaxation dynamics is either controlled by the transverse anisotropy present in the easy (XY) plane or field-induced phonon bottleneck effect of the direct relaxation of the ground KDs. Also, the direct process is represented with a high anisotropic system setting aside the sign of the D parameters. In addition, the experimental and theoretical results for the said complex deduce that the relaxation dynamics are mainly controlled by the transverse anisotropy. To gain more understanding about the magnetization reversal process, we have studied the average relaxation time at 4 K in a different external field. For this, eq 2 was used, where the first term represents the field dependence process (QTM process) and the second term, the weak field dependence (Raman and Orbach process), which is kept as constant. Since the average relaxation time increases with field (Figure S15), the direct term contribution was neglected for the studied complexes.^{11a}

$$\tau^{-1} = B_1/(1 + B_2 H^2) + C \quad (2)$$

The relaxation times were found to be in conjecture (Figure S15) with eq 2 (τ_{QTM} was calculated as 1.9×10^{-4} s for 1 and 2.2×10^{-4} s for 2), which further signifies that QTM has a sizable effect on the slow relaxation process. Additionally, by considering the thermally activated process (either Orbach or Raman), the temperature dependence of τ at 0.2 T can be modeled well (Figure S15) by the power law as eq 3 (where τ_{QTM} was fixed as 1.9×10^{-4} s (1) and 2.2×10^{-4} s (2), $n = 4.9$ (1), 4.6 (2)), which indicates QTM has been well suppressed. The values of n in the range of $n = 1$ –6 also suggest the possibility of spin–lattice relaxation through the admixture of

single phonon direct and optical acoustic Raman processes as reported by Colacio et al.¹⁸

$$\tau^{-1} = \tau_{\text{QTM}}^{-1} + bT^n \quad (3)$$

Moreover, from both field and temperature dependence of the relaxation time, it is obvious that QTM plays a major role in the slow relaxation process. Also, thermal dependence like an optical or acoustic Raman pathway is also important. Additionally, to examine the effect of dipolar interaction on the slow magnetic relaxation process, we have prepared diluted compounds for complexes **1**, **2**, and **3** to obtain **1a**, **2a**, and **3a**, respectively, by using the mixture of $\text{Co}(\text{ClO}_4)_2 \cdot 6\text{H}_2\text{O}$ and $\text{Zn}(\text{ClO}_4)_2 \cdot 6\text{H}_2\text{O}$ in a 5:95 percentage ratio. The presence of Zn and Co elements and a doped level in the diluted samples were verified by energy dispersive X-ray spectroscopy (EDS; Figures S16, S17, and S18). The compounds **1a** and **2a** show the temperature dependence of out-of-phase susceptibility (Figure S19) at little higher temperature range (2–5.9 K for **1a** and 2–4.8 K for **2a**) as compared to **1** (2.0–5.2 K) and **2** (2.0–4.3 K) under the same external field. But no such difference was found in ac susceptibilities for **3a** (Figure S19). Thus, it can be specified that in **1** and **2** the dipolar interaction plays a role in the slow relaxation process, which does not arise from the single ion anisotropy.

We have computed energy levels of the lowest two KDs using the SINGLE_ANISO module by MOLCAS (Figures 7

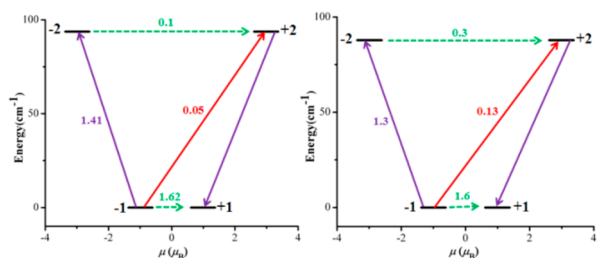


Figure 7. Single_Aniso computed relaxation mechanism for complexes **1** (left) and **2** (right). Black, green, blue, and red line represent KDs, QTM, TA-QTM, and Orbach processes, respectively.

and S20). The computed energies of first excited states are relatively higher (Table S10) as compared to the observed energy barrier, which further suggests that the Orbach process is not playing a major role for all complexes. In addition, the matrix elements of the transition magnetic moment between the states +1 and -1 are quite high (Figures 7 and S20) suggesting a strong QTM present in the ground KDs, which quenched the magnetization and makes it impossible to show zero field SIMs behavior for all the complexes.

Although the solvent molecules coordinate to all the complexes, in **1** and **2** they are also present in the crystal lattice, which makes a dramatic change in the crystal packing, which makes a dramatic change in the crystal packing. The large difference in relaxation dynamics between complexes **1** and **2** and complex **3** may not be possible only because of the coordinating solvent. As in the first coordination sphere, the metal-solvent bond distances are almost similar in all complexes. On the other hand, distortion and the axial O1–Co–O2 bond angle between **1** and **3** both are in distorted PBP geometry, whereas **2** is in almost perfect PBP geometry. Thus, bond distances and local symmetry of all the complexes suggest that crystal field effects may not be responsible for different relaxation dynamics. It further consisted of theoret-

ically obtained D values as calculated without solvent molecules, which are almost same for all the complexes. At the same time, the lattice solvent molecules are also involved in several noncovalent interactions which lead to the formation of different assemblies at low temperatures. These assemblies also may help for slower spin relaxation than the pure mononuclear system where such interactions are absent. On the other hand, the dilution study reveals that dipolar interaction has an important role in the slow relaxation process in **1** and **2**, whereas no such behavior is observed in **3**. The presence of solvent in the crystal lattice results in different crystal packing as well as supramolecular reorganization which further affect the orientation of the anisotropic axis. In addition, the experimentally observed different transverse anisotropy parameters (E) caused by the dipole–dipole interactions, which also tune the relaxation rate, arise from the incoherent QTM.^{12f} Probably, the different crystal packing/supramolecular arrangements and the dipole–dipole interactions are responsible for different relaxation dynamics in all the complexes.^{12b,g} Additionally, we have done thermal analysis (Figure S21) for complex **1** and **2**, which indicates the loss of lattice and coordinated solvent molecules. Thus, we are unable to measure the magnetic data for the desolvated samples.

CONCLUSION

In summary, we have shown three hepta-coordinated Co^{II} complexes with different relaxation dynamics because of the lattice solvent molecules. The noncovalent interactions caused by the lattice solvent molecules lead to different supramolecular reorganization, which further has a dramatic effect to alter the magnetic behavior of the complexes. Solvent molecules are present in both **1** and **2**, which show field induced SIM behavior above 2 K with $U_{\text{eff}} = 25$ and 15 K, whereas due to the absence of the solvent molecule in **3** ($U_{\text{eff}} = 4$ K), no peak maxima are observed above 2 K. In all the complexes, it has also been observed that QTM through the ground states is the major relaxation process, and thermal dependence also makes it clear that an optical or acoustic Raman pathway is important too.

EXPERIMENTAL SECTION

Materials and General Procedure. All the chemicals and reagents were analytical grade and used without further purification. The magnetic susceptibilities were measured by a Quantum Design SQUID-VSM magnetometer. The sample holder correction was done for the experimental measure values, and the magnetic susceptibilities were calculated after diamagnetic correction estimated from Pascal's table.¹⁹ Elemental analysis was performed on an Elemental Microvario Cube Elemental Analyzer. The IR spectrum was recorded on KBr pellets using a PerkinElmer spectrometer. Powder X-ray diffraction (PXRD) data were collected on a PANalytical EMPYR-EAN instrument using $\text{Cu K}\alpha$ radiation.

Crystal Data Collection and Structure Determination. Intensity data were collected on a Bruker APEX-II CCD diffractometer using graphite monochromated $\text{Mo K}\alpha$ radiation ($\alpha = 0.71073 \text{ \AA}$) at 140 K. Data collections were performed using a φ and ω scan. All the structures were solved using the ShelXT^{20,21} structure solution program using intrinsic phrasing, and olex2²² was used as the graphical interface. The models were refined with ShelXL²³ with full matrix least-squares minimization on F^2 . All non-hydrogen atoms were refined anisotropically. Crystallographic data of complexes **1**, **2**, and **3** have been summarized in Table S1

Computational Details (ORCA and MOLCAS 8.2). All the calculations have been performed with the ORCA 4.0 and MOLCAS 8.2 software packages. The coordinates obtained from single crystal X-

ray structure were used without optimization. In ORCA, we have used ZORA (zeroth-order regular approximation) throughout the calculation. The def2-TZVPP basis set was used for Co and def-SV(P) for other atoms in combination with auxiliary basis set def2/JK. In the active space, we have considered seven electrons in 5 d orbital CAS (5,7), and in the CI configuration (configuration interaction) procedure, 10 quartets and 40 doublets were computed. Further, to consider the dynamic correlation effects, N-electron valence perturbation theory (NEVPT2) was included on top of the CASSCF wave function. Also we employed the quasi-degenerate perturbation theory (QDPT)^{24,25} approach for spin-orbit coupling effects. Both the second order perturbation theory and an effective Hamiltonian approach (EHA)²⁶ have been used to estimate the ZFS parameters *D* and *E*. In MOLCAS, the calculations of the CASSCF/RASSI-SO/SINGLE_ANISO type and the ANO-RCC basis set of the function have been used for all the atoms ([ANO-RCC-VTZP] for Co, [ANO-RCC-VTZ] for O and N, and [ANO-RCC-VDZ] for C and H) with relativistic effects using the Douglas-Kroll-Hess Hamiltonian.²⁷ In active space, we consider that, similar to the previous calculation, [CAS(5,7)] and the RASSI program²⁸ have been used to include the spin-orbit coupling effects with the mixed optimized states in previous calculations (10 spin quartet and 40 spin doublet states). SINGLE_ANISO²⁹ was used to compute the anisotropy of the low lying states using *ab initio* wave function and spin-orbit eigenstates.

Synthesis of the Ligand (H₄L). The ligand was synthesized using a simple Schiff base condensation between 2,6-diacetylpyridine and 4-phenylesemicarbazide. To a solution of 2,6-diacetylpyridine (1 mmol, 163 mg) dissolved in 10 mL of ethanol under hot conditions, ethanolic solution (10 mL) of 4-phenylesemicarbazide (2 mmol, 310 mg) was added. Further, four to six drops of glacial acetic acid were added to the solution and the stirring continued under refluxed conditions for 4 h. After cooling to room temperature, a pure white microcrystalline product was obtained and the solution filtered. The precipitate was washed with cold ethanol three to five times and dried under a vacuum, which results in white powder as a pure product. The ligand was used without further purification.

Synthesis of [Co(H₄L)(DMF)(H₂O)](NO₃)₂(DMF) (1). H₄L (0.1 mmol, 42 mg) was added to the 5 mL of acetone, and after few minutes of stirring, Co(NO₃)₂·6H₂O (0.1 mmol, 29 mg) was added at room temperature. The stirring was continued for the next 3 h at 50 °C. A brown yellowish precipitate (ppt) was formed and the reaction mixture cooled to room temperature. After the filtration, the ppt was washed with acetone and dried under a vacuum. Then, the ppt was dissolved in hot DMF solvent and cooled to room temperature. The resultant solution was then kept for vapor diffusion by using diethyl ether (DEE). After 3 days, orange color blocked shaped crystals suitable for X-ray were obtained (yield 70%). Anal. Calcd for C₂₉H₃₉CoN₁₁O₁₁: C, 44.85; H, 5.06; N, 19.84%. Found: C, 45.01; H, 5.02; N, 19.95%. IR (KBr pellet, 4000–400 cm⁻¹), ν /cm⁻¹: 3233, 3090, 3047, 2982, 2962, 1537, 1383, 1333, 1261, 1107, 1040, 756.

Synthesis of [Co(H₄L)(MeOH)(H₂O)](NO₃)₂(MeOH) (2). The ligand (0.1 mmol, 42 mg) was added in 3 mL of methanol solvent and the solution stirred for 15 min. The methanolic solution of Co(NO₃)₂·6H₂O (0.1 mmol, 29 mg in 3 mL of MeOH) was then slowly added to the ligand solution and the solution stirred for 4 h at 60 °C. The solution was cooled at room temperature and filtered, and the filtrate was kept for slow evaporation. Brown colored block shaped crystals were obtained after 4 days and washed with Et₂O (yield 90%). Anal. Calcd for C₂₅H₃₃CoN₉O₁₁: C, 43.23; H, 4.79; N, 18.15%. Found: C, 43.37; H, 4.84; N, 18.19%. IR (KBr pellet, 4000–400 cm⁻¹), ν /cm⁻¹: 3198, 3098, 2944, 2826, 1569, 1383, 1329, 1261, 1095, 1034, 759.

Synthesis of [Co(H₄L)(DEF)(H₂O)](NO₃)₂ (3). Complex 3 was synthesized according to a procedure similar to that of complex 1. In this case, the obtained precipitate from acetone solution was dissolved in DEF solvent (yield 60%). Anal. Calcd for C₂₈H₃₆CoN₁₀O₁₀: C, 45.97; H, 4.96; N, 19.15%. Found: C, 46.01; H, 5.03; N, 19.21%. IR (KBr pellet, 4000–400 cm⁻¹), ν /cm⁻¹: 3245, 3037, 2973, 2876, 1570, 1384, 1335, 1296, 1053, 1037, 756.

Preparation of Diluted Sample. The diluted sample has been prepared using a method similar to that for complexes 1, 2, and 3; however, a mixture of Zn(ClO₄)₂·6H₂O and Co(ClO₄)₂·6H₂O in a 95:5 percentage ratio was used.

■ ASSOCIATED CONTENT

📄 Supporting Information

The Supporting Information is available free of charge on the ACS Publications website at DOI: 10.1021/acs.inorgchem.9b00615.

It includes PXRD, plots, and additional data of magnetic characterizations (PDF)

Accession Codes

CCDC 1895210–1895212 contain the supplementary crystallographic data for this paper. These data can be obtained free of charge via www.ccdc.cam.ac.uk/data_request/cif, or by emailing data_request@ccdc.cam.ac.uk, or by contacting The Cambridge Crystallographic Data Centre, 12 Union Road, Cambridge CB2 1EZ, UK; fax: +44 1223 336033.

■ AUTHOR INFORMATION

Corresponding Author

*Tel.: +91-755-6691313. E-mail: skonar@iiserb.ac.in.

ORCID

Sanjit Konar: 0000-0002-1584-6258

Notes

The authors declare no competing financial interest.

■ ACKNOWLEDGMENTS

We thank Dr. Subhadip Roy for his valuable and scientific support. A.M. thanks IISER Bhopal for the SRF fellowship. A.K.H. thanks CSIR for the SRF fellowship, and S.K. thanks CSIR (Project No. 01(2974)/19/EMR-II) Government of India and IISER Bhopal for generous financial support.

■ REFERENCES

- (1) Sessoli, R.; Gatteschi, D.; Caneschi, A.; Novak, M. A. Magnetic bistability in a metal-ion cluster. *Nature* **1993**, *365*, 141–143.
- (2) Bogani, L.; Wernsdorfer, W. Molecular spintronics using single-molecule magnets. *Nat. Mater.* **2008**, *7*, 179–186.
- (3) (a) Santini, P.; Carretta, S.; Troiani, F.; Amoretti, G. Molecular Nanomagnets as Quantum Simulators. *Phys. Rev. Lett.* **2011**, *107*, 230502. (b) Timco, G. A.; Faust, T. B.; Tuna, F.; Winpenny, R. E. P. Linking heterometallic rings for quantum information processing and amusement. *Chem. Soc. Rev.* **2011**, *40*, 3067–3075. (c) Furrer, A.; Waldmann, O. Magnetic cluster excitations. *Rev. Mod. Phys.* **2013**, *85*, 367–420. (d) Timco, G. A.; McInnes, E. J. L.; Winpenny, R. E. P. Physical studies of heterometallic rings: an ideal system for studying magnetically-coupled systems. *Chem. Soc. Rev.* **2013**, *42*, 1796–1806.
- (4) (a) Sessoli, R.; Tsai, H. L.; Schake, A. R.; Wang, S.; Vincent, J. B.; Folting, K.; Gatteschi, D.; Christou, G.; Hendrickson, D. N. High-spin molecules: [Mn₁₂O₁₂(O₂CR)₁₆(H₂O)₄]. *J. Am. Chem. Soc.* **1993**, *115*, 1804–1816. (b) Ako, A. M.; Hewitt, I. J.; Mereacre, V.; Clérac, R.; Wernsdorfer, W.; Anson, C. E.; Powell, A. K. A Ferromagnetically Coupled Mn₁₉ Aggregate with a Record S = 83/2 Ground Spin State. *Angew. Chem.* **2006**, *118*, 5048–5051. (c) Milios, C. J.; Vinslava, A.; Wernsdorfer, W.; Moggach, S.; Parsons, S.; Perlepes, S. P.; Christou, G.; Brechin, E. K. A Record Anisotropy Barrier for a Single-Molecule Magnet. *J. Am. Chem. Soc.* **2007**, *129*, 2754–2755. (d) Maheswaran, S.; Chastanet, G.; Teat, S. J.; Mallah, T.; Sessoli, R.; Wernsdorfer, W.; Winpenny, R. E. P. Phosphonate ligands stabilize mixed-valent {Mn^{III}₂₀·MnII_x} clusters with large spin and coercivity. *Angew. Chem., Int. Ed.* **2005**, *44*, 5044–5048.

- (5) (a) Liu, J.; Chen, Y.-C.; Liu, J.-L.; Vieru, V.; Ungur, L.; Jia, J.-H.; Chibotaru, L. F.; Lan, Y.; Wernsdorfer, W.; Gao, S.; Chen, X.-M.; Tong, M.-L. A Stable Pentagonal Bipyramidal Dy(III) Single-Ion Magnet with a Record Magnetization Reversal Barrier over 1000 K. *J. Am. Chem. Soc.* **2016**, *138*, 5441–5450. (b) Goodwin, C. A. P.; Ortu, F.; Reta, D.; Chilton, N. F.; Mills, D. P. Molecular magnetic hysteresis at 60 K in dysprosocenium. *Nature* **2017**, *548*, 439–442. (c) Sessoli, R. Magnetic molecules back in the race. *Nature* **2017**, *548*, 400–401. (d) Chen, Y.-C.; Liu, J.-L.; Wernsdorfer, W.; Liu, D.; Chibotaru, L. F.; Chen, X.-M.; Tong, M.-L. Hyperfine Interaction Driven Suppression of Quantum Tunneling at Zero Field in a Holmium(III) Single Ion Magnet. *Angew. Chem., Int. Ed.* **2017**, *56*, 4996–5000. (e) Gupta, S. K.; Rajeshkumar, T.; Rajaraman, G.; Murugavel, R. An unprecedented zero field neodymium(III) single-ion magnet based on a phosphonidamide. *Chem. Commun.* **2016**, *52*, 7168–7171. (f) Guo, F.-S.; Day, B. M.; Chen, Y.-C.; Tong, M.-L.; Mansikkamäki, A.; Layfield, R. A. Magnetic hysteresis up to 80 K in a dysprosium metallocene single-molecule magnet. *Science* **2018**, *362*, 1400–1403.
- (6) (a) Gogoi, N.; Thlijeni, M.; Duhayon, C.; Sutter, J. P. Heptacoordinated Nickel(II) as an Ising-Type Anisotropic Building Unit: Illustration with a Pentanuclear $[(NiL)_3\{W(CN)_8\}_2]$ Complex. *Inorg. Chem.* **2013**, *52*, 2283–2285. (b) Zadrozny, J. M.; Atanasov, M.; Bryan, A. M.; Lin, C. Y.; Rekker, B. D.; Power, P. P.; Neese, F.; Long, J. R. Slow magnetization dynamics in a series of two-coordinate iron(II) complexes. *Chem. Sci.* **2013**, *4*, 125–138. (c) Singh, S. K.; Gupta, T.; Badkur, P.; Rajaraman, G. Magnetic Anisotropy of Mononuclear Ni^{II} Complexes: On the Importance of Structural Diversity and the Structural Distortions. *Chem. - Eur. J.* **2014**, *20*, 10305–10313. (d) Mossin, S.; Tran, B. L.; Adhikari, D.; Pink, M.; Heinemann, F. M.; Sutter, J.; Szilagy, R. K.; Meyer, K.; Mendiola, D. J. A Mononuclear Fe(III) Single Molecule Magnet with a $3/2 \leftrightarrow 5/2$ Spin Crossover. *J. Am. Chem. Soc.* **2012**, *134*, 13651–13661. (e) Ruamps, R.; Maurice, R.; Batchelor, L.; Boggio-Pasqua, M.; Guillot, R.; Barra, A. L.; Liu, J. J.; Bendeif, E.; Pillet, S.; Hill, S.; Mallah, T.; Guihéry, N. Giant Ising-Type Magnetic Anisotropy in Trigonal Bipyramidal Ni(II) Complexes: Experiment and Theory. *J. Am. Chem. Soc.* **2013**, *135*, 3017–3026. (f) Karunadasa, H. L.; Arquero, K. D.; Berben, L. A.; Long, J. R. Enhancing the Magnetic Anisotropy of Cyano-Ligated Chromium(II) and Chromium(III) Complexes via Heavy Halide Ligand Effects. *Inorg. Chem.* **2010**, *49*, 4738–4740. (g) Mathonière, C.; Lin, H.-J.; Siretanu, D.; Clérac, R.; Smith, J. M. Photoinduced Single-Molecule Magnet Properties in a Four-Coordinate Iron(II) Spin Crossover Complex. *J. Am. Chem. Soc.* **2013**, *135*, 19083–19086. (h) Murrie, M. Cobalt(II) single-molecule magnets. *Chem. Soc. Rev.* **2010**, *39*, 1986–1995. (i) Goswami, S.; Mondal, A. K.; Konar, S. Nanoscopic molecular magnets. *Inorg. Chem. Front.* **2015**, *2*, 687–712. (j) Frost, J. M.; Harriman, K. L. M.; Murugesu, M. The rise of 3-d single-ion magnets in molecular magnetism: towards materials from molecules? *Chem. Sci.* **2016**, *7*, 2470–2491. (k) Gómez-Coca, S.; Cremades, E.; Aliaga-Alcalde, N.; Ruiz, E. Mononuclear Single-Molecule Magnets: Tailoring the Magnetic Anisotropy of First-Row Transition-Metal Complexes. *J. Am. Chem. Soc.* **2013**, *135*, 7010–7018. (l) Rajnák, C.; Titiš, J.; Fuhr, O.; Ruben, M.; Boča, R. Single-Molecule Magnetism in a Pentacoordinate Cobalt(II) Complex Supported by an Antenna Ligand. *Inorg. Chem.* **2014**, *53*, 8200–8202.
- (7) (a) Ruamps, R.; Batchelor, L. J.; Guillot, R.; Zakhia, G.; Barra, A.-L.; Wernsdorfer, W.; Guihéry, N.; Mallah, T. Ising-type magnetic anisotropy and single molecule magnet behaviour in mononuclear trigonal bipyramidal Co(II) complexes. *Chem. Sci.* **2014**, *5*, 3418–3424. (b) Rajnák, C.; Titiš, J.; Fuhr, O.; Ruben, M.; Boča, R. Single-Molecule Magnetism in a Pentacoordinate Cobalt(II) Complex Supported by an Antenna Ligand. *Inorg. Chem.* **2014**, *53*, 8200–8202. (c) Smolkó, L.; Černák, J.; Dušek, M.; Miklovič, J.; Titiš, J.; Boča, R. Three tetracoordinate Co(II) complexes $[Co(biq)X_2]$ ($X = Cl, Br, I$) with easy-plane magnetic anisotropy as field-induced single-molecule magnets. *Dalton Trans* **2015**, *44*, 17565–17571. (d) Zhang, Y.-Z.; Gómez-Coca, S.; Brown, A. J.; Saber, M. R.; Zhang, X.; Dunbar, K. R. Trigonalantiprismatic Co(II) single molecule magnets with large uniaxial anisotropies: importance of Raman and tunneling mechanisms. *Chem. Sci.* **2016**, *7*, 6519–6527. (e) Vallejo, J.; Castro, I.; Ruiz-García, R.; Cano, J.; Julve, M.; Lloret, F.; De Munno, G.; Wernsdorfer, W.; Pardo, E. Field-Induced Slow Magnetic Relaxation in a Six-Coordinate Mononuclear Cobalt(II) Complex with a Positive Anisotropy. *J. Am. Chem. Soc.* **2012**, *134*, 15704–15707. (f) Mondal, A. K.; Jover, J.; Ruiz, E.; Konar, S. Investigation of easy-plane magnetic anisotropy in P-ligand square-pyramidal Co^{II} single ion magnets. *Chem. Commun.* **2017**, *53*, 5338–5341. (g) Craven, M.; Nygaard, M. H.; Zadrozny, J. M.; Long, J. R.; Overgaard, J. Determination of d-Orbital Populations in a Cobalt(II) Single-Molecule Magnet Using Single-Crystal X-ray Diffraction. *Inorg. Chem.* **2018**, *57*, 6913–6920. (h) Yao, B.; Deng, Y.-F.; Li, T.; Xiong, J.; Wang, B.-W.; Zheng, Z.; Zhang, Y.-Z. Construction and Magnetic Study of a Trigonal-Prismatic Cobalt(II) Single-Ion Magnet. *Inorg. Chem.* **2018**, *57*, 14047–14051. (i) Switlicka, A.; Machura, B.; Penkala, M.; Bieńko, A.; Bieńko, D. C.; Titiš, J.; Rajnák, C.; Boča, R.; Ozarowski, A.; Ozerov, M. Slow Magnetic Relaxation in Cobalt(II) Field-Induced Single-Ion Magnets with Positive Large Anisotropy. *Inorg. Chem.* **2018**, *57*, 12740–12755. (j) Pavlov, A. A.; Savkina, S. A.; Belov, A. S.; Nelyubina, Y. V.; Efimov, N. N.; Voloshin, Y. Z.; Novikov, V. V. Trigonal Prismatic Tris-pyridineoximate Transition Metal Complexes: A Cobalt(II) Compound with High Magnetic Anisotropy. *Inorg. Chem.* **2017**, *56*, 6943–6951. (k) Tong, J.; Demeshko, S.; John, M.; Dechert, S.; Meyer, F. Redox-Induced Single-Molecule Magnetism in Mixed-Valent $[2 \times 2] Co_4$ Grid Complexes. *Inorg. Chem.* **2016**, *55*, 4362–4372. (l) Vaidya, S.; Tewary, S.; Singh, S. K.; Langley, S. K.; Murray, K. S.; Lan, Y.; Wernsdorfer, W.; Rajaraman, G.; Shanmugam, M. What Controls the Sign and Magnitude of Magnetic Anisotropy in Tetrahedral Cobalt(II) Single-Ion Magnets? *Inorg. Chem.* **2016**, *55*, 9564–9578. (m) Boča, R.; Rajnák, C.; Moncol, J.; Titiš, J.; Valigura, D. Breaking the Magic Border of One Second for Slow Magnetic Relaxation of Cobalt-Based Single Ion Magnets. *Inorg. Chem.* **2018**, *57*, 14314–14321.
- (8) (a) Yao, X.-N.; Du, J.-Z.; Zhang, Y.-Q.; Leng, X.-B.; Yang, M.-W.; Jiang, S.-D.; Wang, Z.-X.; Ouyang, Z.-W.; Deng, L.; Wang, B.-W.; Gao, S. Two-Coordinate Co(II) Imido Complexes as Outstanding Single-Molecule Magnets. *J. Am. Chem. Soc.* **2017**, *139*, 373–380. (b) Rechkemmer, Y.; Breitgoff, F. D.; van der Meer, M.; Atanasov, M.; Hakl, M.; Orlita, M.; Neugebauer, P.; Neese, F.; Sarkar, B.; van Slageren, J. A four-coordinate cobalt(II) single-ion magnet with coercivity and a very high energy barrier. *Nat. Commun.* **2016**, *7*, 1046. (c) Bunting, P. C.; Atanasov, M.; Damgaard-Møller, E.; Perfetti, M.; Crassee, L.; Orlita, M.; Overgaard, J.; van Slageren, J.; Neese, F.; Long, J. R. A linear cobalt(II) complex with maximal orbital angular momentum from a non-Aufbau ground state. *Science* **2018**, *362*, No. eaat7319. (d) Meng, Y.-S.; Mo, Z.; Wang, B.-W.; Zhang, Y.-Q.; Deng, L.; Gao, S. Observation of the single-ion magnet behavior of d^8 ions on two-coordinate Co(i)–NHC complexes. *Chem. Sci.* **2015**, *6*, 7156–7162.
- (9) (a) Sun, W.-B.; Yan, P.-F.; Jiang, S.-D.; Wang, B.-W.; Zhang, Y.-Q.; Li, H.-F.; Chen, P.; Wang, Z.-M.; Gao, S. High symmetry or low symmetry, that is the question - high performance Dy(III) single-ion magnets by electrostatic potential design. *Chem. Sci.* **2016**, *7*, 684–691. (b) Ding, Y.-S.; Chilton, N. F.; Winpenny, R. E. P.; Zheng, Y.-Z. On Approaching the Limit of Molecular Magnetic Anisotropy: A Near Perfect Pentagonal Bipyramidal Dysprosium(III) Single Molecule Magnet. *Angew. Chem., Int. Ed.* **2016**, *55*, 16071–16074. (c) Gregson, M.; Chilton, N. F.; Ariciu, A.-M.; Tuna, F.; Crowe, I. F.; Lewis, W.; Blake, A. J.; Collison, D.; McInnes, E. J. L.; Winpenny, R. E. P.; Liddle, S. T. A monometallic lanthanide bis(methanediide) single molecule magnet with a large energy barrier and complex spin relaxation behaviour. *Chem. Sci.* **2016**, *7*, 155–165. (d) Liu, J.-L.; Chen, Y.-C.; Zheng, Y.-Z.; Lin, W.-Q.; Ungur, L.; Wernsdorfer, W.; Chibotaru, L. F.; Tong, M.-L. Switching the anisotropy barrier of a single-ion magnet by symmetry change from quasi- D_{2h} to quasi-Oh. *Chem. Sci.* **2013**, *4*, 3310–3316. (e) Liu, J.; Chen, Y.-C.; Liu, J.-L.; Vieru, V.; Ungur, L.; Jia, J.-H.; Chibotaru, L. F.; Lan, Y.; Wernsdorfer,

- W.; Gao, S.; Chen, X.-M.; Tong, M.-L. A Stable Pentagonal Bipyramidal Dy(III) Single-Ion Magnet with a Record Magnetization Reversal Barrier over 1000 K. *J. Am. Chem. Soc.* **2016**, *138*, 5441–5450. (f) Chen, Y.-C.; Liu, J.-L.; Wernsdorfer, W.; Liu, D.; Chibotaru, L. F.; Chen, X.-M.; Tong, M.-L. Hyperfine Interaction Driven Suppression of Quantum Tunneling at Zero Field in a Holmium(III) Single Ion Magnet. *Angew. Chem., Int. Ed.* **2017**, *56*, 4996–5000. (g) Gupta, S. K.; Rajeshkumar, T.; Rajaraman, G.; Murugavel, R. Is a strong axial crystal-field the only essential condition for a large magnetic anisotropy barrier? The case of non-Kramers Ho(III) versus Tb(III). *Dalton Trans* **2018**, *47*, 357–366.
- (10) (a) Drahoš, B.; Herchel, R.; Trávníček, Z. Impact of Halogenido Coligands on Magnetic Anisotropy in Seven-Coordinate Co(II) Complexes. *Inorg. Chem.* **2017**, *56*, 5076–5088. (b) Antal, P.; Drahoš, B.; Herchel, R.; Trávníček, Z. Late First-Row Transition-Metal Complexes Containing a 2-Pyridylmethyl Pendant-Armed 15-Membered Macrocyclic Ligand. Field-Induced Slow Magnetic Relaxation in a Seven-Coordinate Cobalt(II) Compound. *Inorg. Chem.* **2016**, *55*, 5957–5972. (c) Shao, D.; Zhang, S.-L.; Shi, L.; Zhang, Y.-Q.; Wang, X.-Y. Probing the Effect of Axial Ligands on Easy-Plane Anisotropy of Pentagonal-Bipyramidal Cobalt(II) Single-Ion Magnets. *Inorg. Chem.* **2016**, *55*, 10859–10869. (d) Dey, M.; Dutta, S.; Sarma, B.; Deka, R. C.; Gogoi, N. Modulation of Coordination Environment: A Convenient Approach to Tailor Magnetic Anisotropy in Seven Coordinate Co(II) Complexes. *Chem. Commun.* **2016**, *52*, 753–756. (e) Mondal, A. K.; Mondal, A.; Dey, B.; Konar, S. Influence of the Coordination Environment on Easy-Plane Magnetic Anisotropy of Pentagonal Bipyramidal Cobalt(II) Complexes. *Inorg. Chem.* **2018**, *57*, 9999–10008.
- (11) (a) Mondal, A. K.; Goswami, T.; Misra, A.; Konar, S. Probing the Effects of Ligand Field and Coordination Geometry on Magnetic Anisotropy of Pentacoordinate Cobalt(II) Single-Ion Magnets. *Inorg. Chem.* **2017**, *56*, 6870–6878. (b) Mondal, A. K.; Sundarajan, M.; Konar, S. A new series of tetrahedral Co(ii) complexes [CoL₂X₂] (X = NCS, Cl, Br, I) manifesting single-ion magnet features. *Dalton Trans* **2018**, *47*, 3745–3754. (c) Mondal, A. K.; Jover, J.; Ruiz, E.; Konar, S. Single-ion magnetic anisotropy in a vacant octahedral Co(ii) complex. *Dalton Trans* **2019**, *48*, 25–29. (d) Mondal, A. K.; Jover, J.; Ruiz, E.; Konar, S. Quantitative Estimation of Ising-Type Magnetic Anisotropy in a Family of C₃-Symmetric CoII Complexes. *Chem. - Eur. J.* **2017**, *23*, 12550–12558. (e) Mondal, A. K.; Khatua, S.; Tomar, K.; Konar, S. Field-Induced Single-Ion-Magnetic Behavior of Octahedral CoII in a Two-Dimensional Coordination Polymer. *Eur. J. Inorg. Chem.* **2016**, *2016*, 3545–3552.
- (12) (a) Zhang, W.-Y.; Zhang, Y.-Q.; Jiang, S.-D.; Sun, W.-B.; Li, H.-F.; Wang, B.-W.; Chen, P.; Yan, P.-F.; Gao, S. Dramatic impact of the lattice solvent on the dynamic magnetic relaxation of dinuclear dysprosium single-molecule magnets. *Inorg. Chem. Front.* **2018**, *5*, 1575–1586. (b) Zhang, X.; Vieru, V.; Feng, X.; Liu, J.-L.; Zhang, Z.; Na, B.; Shi, W.; Wang, B.-W.; Powell, A. K.; Chibotaru, L. F.; Gao, S.; Cheng, P.; Long, J. R. Influence of Guest Exchange on the Magnetization Dynamics of Dilanthanide Single-Molecule-Magnet Nodes within a Metal–Organic Framework. *Angew. Chem., Int. Ed.* **2015**, *54*, 9861–9865. (c) Ren, M.; Pinkowicz, D.; Yoon, M.; Kim, K.; Zheng, L.-M.; Breedlove, B. K.; Yamashita, M. Dy(III) Single-Ion Magnet Showing Extreme Sensitivity to (De)hydration. *Inorg. Chem.* **2013**, *52*, 8342–8348. (d) Liu, J.; Zhang, X.-P.; Wu, T.; Ma, B.-B.; Wang, T.-W.; Li, C.-H.; Li, Y.-Z.; You, X.-Z. Solvent-Induced Single-Crystal-to-Single-Crystal Transformation in Multifunctional Chiral Dysprosium(III) Compounds. *Inorg. Chem.* **2012**, *51*, 8649–8651. (e) Peng, Y.; Mereacre, V.; Anson, C. E.; Powell, A. K. The role of coordinated solvent on Co(ii) ions in tuning the single molecule magnet properties in a {Co^{II}₂Dy^{III}₂} system. *Dalton Trans* **2017**, *46*, 5337–5343. (f) Zhang, S.; Ke, H.; Sun, L.; Li, X.; Shi, Q.; Xie, G.; Wei, Q.; Yang, D.; Wang, W.; Chen, S. Magnetization Dynamics Changes of Dysprosium(III) Single-Ion Magnets Associated with Guest Molecules. *Inorg. Chem.* **2016**, *55*, 3865–3871. (g) Bi, Y.; Guo, Y.-N.; Zhao, L.; Guo, Y.; Lin, S.-Y.; Jiang, S.-D.; Tang, J.; Wang, B.-W.; Gao, S. Capping Ligand Perturbed Slow Magnetic Relaxation in Dysprosium Single-Ion Magnets. *Chem. - Eur. J.* **2011**, *17*, 12476–12481.
- (13) Alvarez, S.; Alemany, P.; Casanova, D.; Cirera, J.; Llunell, M.; Avnir, D. Shape Maps and Polyhedral Interconversion Paths in Transition Metal Chemistry. *Coord. Chem. Rev.* **2005**, *249*, 1693–1708.
- (14) Chilton, N. F.; Anderson, R. P.; Turner, L. D.; Soncini, A.; Murray, K. S. PHI: A powerful new program for the analysis of anisotropic monomeric and exchange-coupled polynuclear- and f-block complexes. *J. Comput. Chem.* **2013**, *34*, 1164–1175.
- (15) Neese, F. The ORCA program system. *Wiley Interdiscip. Rev.: Comput. Mol. Sci.* **2012**, *2*, 73–78.
- (16) Aquilante, F.; De Vico, L.; Ferré, N.; Ghigo, G.; Malmqvist, P.-Å.; Neogrády, P.; Pedersen, T. B.; Pitoňák, M.; Reiher, M.; Roos, B. O.; Serrano-Andrés, L.; Urban, M.; Veryazov, V.; Lindh, R. MOLCAS 7: The Next Generation. *J. Comput. Chem.* **2010**, *31*, 224–247.
- (17) (a) Cole, K. S.; Cole, R. H. Dispersion and Absorption in Dielectrics I. Alternating Current Characteristics. *J. Chem. Phys.* **1941**, *9*, 341. (b) Guo, Y.-N.; Xu, G.-F.; Guo, Y.; Tang, J. Relaxation dynamics of dysprosium(III) single molecule magnets. *Dalton Trans* **2011**, *40*, 9953–9963.
- (18) Colacio, E.; Ruiz, J.; Ruiz, E.; Cremades, E.; Krzystek, J.; Carretta, S.; Cano, J.; Guidi, T.; Wernsdorfer, W.; Brechin, E. K. Slow magnetic relaxation in a Co(II)-Y(III) single-ion magnet with positive axial zero-field splitting. *Angew. Chem., Int. Ed.* **2013**, *52*, 9130–9143.
- (19) Kahn, O. *Molecular Magnetism*; VCH Publishers Inc., 1991.
- (20) Dolomanov, O. V.; Bourhis, L. J.; Gildea, R. J. J.; Howard, A. K.; Puschmann, H. A complete structure solution, refinement and analysis program. *J. Appl. Crystallogr.* **2009**, *42*, 339–341.
- (21) Sheldrick, G. M. SHELXTL-97, Program for X-ray Crystal Structure Solution; University of Göttingen: Göttingen, Germany, 1997.
- (22) Dolomanov, O. V.; Bourhis, L. J.; Gildea, R. J.; Howard, J. A. K.; Puschmann, H. A complete structure solution, refinement and analysis program. *J. Appl. Crystallogr.* **2009**, *42*, 339–341.
- (23) Sheldrick, G. M. Crystal structure refinement with ShelXL. *Acta Crystallogr., Sect. C: Struct. Chem.* **2015**, *71*, 3–8.
- (24) Ganayushin, D.; Neese, F. First-principles calculations of magnetic circular dichroism spectra. *J. Chem. Phys.* **2008**, *128*, 114117.
- (25) Atanasov, M.; Aravena, D.; Suturina, E.; Bill, E.; Maganas, D.; Neese, F. First principles approach to the electronic structure, magnetic anisotropy and spin relaxation in mononuclear 3d-transition metal single molecule magnets. *Coord. Chem. Rev.* **2015**, *289*, 177–214.
- (26) Maurice, R.; Bastardis, R.; de Graaf, C.; Suaud, N.; Mallah, T.; Guihéry, N. Universal Theoretical Approach to Extract Anisotropic Spin Hamiltonians. *J. Chem. Theory Comput.* **2009**, *5*, 2977–2984.
- (27) Douglas, M.; Kroll, N. M. Quantum electrodynamic corrections to the fine structure of helium. *Ann. Phys.* **1974**, *82*, 89–155. (b) Hess, B. A. Relativistic electronic-structure calculations employing a two-component no-pair formalism with external-field projection operators. *Phys. Rev. A: At, Mol., Opt. Phys.* **1986**, *33*, 3742. (c) Reiher, M. Relativistic Douglas–Kroll–Hess theory. *WIREs Comput. Mol. Sci.* **2012**, *2*, 139–149.
- (28) Malmqvist, P. Å.; Roos, B. O.; Schimmelpfennig, B. The restricted active space (RAS) state interaction approach with spin-orbit coupling. *Chem. Phys. Lett.* **2002**, *357*, 230–240.
- (29) Chibotaru, L. F.; Ungur, L. Ab initio calculation of anisotropic magnetic properties of complexes. I. Unique definition of pseudospin Hamiltonians and their derivation. *J. Chem. Phys.* **2012**, *137*, 064112.